

ASASSN-15jd: WZ Sge-type star with intermediate superoutburst between single and double ones

Mariko KIMURA ^{1,*}, Keisuke ISOGAI ¹, Taichi KATO ¹, Akira IMADA ², Naoto KOJIGUCHI ³, Yuki SUGIURA ³, Daiki FUKUSHIMA ³, Nao TAKEDA ³, Katsura MATSUMOTO ³, Shawn DVORAK ⁴, Tonny VANMUNSTER ⁵, Pavol A. DUBOVSKY ⁶, Igor KUDZEJ ⁶, Ian MILLER ⁷, Elena P. PAVLENKO ⁸, Julia V. BABINA ⁸, Oksana I. ANTONYUK ⁸, Aleksei V. BAKLANOV ⁸, William L. STEIN ⁹, Maksim V. ANDREEV ^{10,11}, Tamás TORDAI ¹², Hiroshi ITOH ¹³, Roger D. PICKARD ^{14,15}, Daisaku NOGAMI ¹
mkimura@kusastro.kyoto-u.ac.jp

¹*Department of Astronomy, Graduate School of Science, Kyoto University, Oiwakecho, Kitashirakawa, Sakyo-ku, Kyoto 606-8502*

²*Kwasan and Hida Observatories, Kyoto University, Yamashina, Kyoto 607-8471*

³*Osaka Kyoiku University, 4-698-1 Asahigaoka, Kashiwara, Osaka 582-8582, Japan*

⁴*Rolling Hills Observatory, 1643 Nightfall Drive, Clermont, Florida 34711, USA*

⁵*Center for Backyard Astrophysics (Belgium), Walhostraat 1A, B-3401, Landen, Belgium*

⁶*Vihorlat Observatory, Mierova 4, Humenne, Slovakia*

⁷*Furzehill House, Ilston, Swansea, SA2 7LE, UK*

⁸*Crimean Astrophysical Observatory, 298409, Nauchny, Republic of Crimea*

⁹*Center for Backyard Astrophysics, 6025 Calle Paraiso, Las Cruces, New Mexico 88012, USA*

¹⁰*Institute of Astronomy, Russian Academy of Sciences, 361605 Peak Terskol, Kabardino-Balkaria, Russia*

¹¹*International Center for Astronomical, Medical and Ecological Research of National Academy of Sciences of Ukraine (NASU), 27 Akademika Zabolotnoho Street, 03680 Kiev, Ukraine*

¹²*Polaris Observatory, Hungarian Astronomical Association, Laborc utca 2/c, 1037 Budapest, Hungary*

¹³*Variable Star Observers League in Japan (VSOLJ), 1001-105 Nishiterakata, Hachioji, Tokyo 192-0153*

¹⁴*The British Astronomical Association, Variable Star Section (BAA VSS), Burlington House, Piccadilly, London, W1J 0DU, UK*

¹⁵*3 The Birches, Shobdon, Leominster, Herefordshire, HR6 9NG, UK*

(Received ; accepted)

Abstract

We present optical photometry of a WZ Sge-type dwarf nova (DN), ASASSN-15jd. Its light curve showed a small dip in the middle of the superoutburst in 2015 for the first time among WZ Sge-type DNe. The unusual light curve implies a delay in the growth of the 3:1 resonance tidal instability. Also, the light curve is similar to those of other two WZ Sge-type stars, SSS J122221.7–311523 and OT J184228.1+483742, which are believed to be the best candidates for a period bouncer on the basis of their small values of the mass ratio ($q \equiv M_2/M_1$). Additionally, the small mean superhump amplitude (< 0.1 mag) and the long duration of no ordinary superhumps at the early stage of the superoutburst are common to the best candidates for a period bouncer. The average superhump period was $P_{\text{sh}} = 0.0649810(78)$ d and no early superhumps were detected. Although we could not estimate the mass ratio of ASASSN-15jd with high accuracy, this object is expected to be a candidate for a period bouncer, a binary accounting for the missing population of post-period minimum cataclysmic variables, based on the above characteristics.

Key words: accretion, accretion disks - novae, cataclysmic variables - stars: dwarf novae - stars: individual (ASASSN-15jd)

1. Introduction

Cataclysmic variables (CVs) are close binary systems composed of a white dwarf (a primary star) and a typical late-type main sequence star (a secondary star). The secondary star fills its Roche lobe and its matter flows toward the primary star via the Roche-lobe overflow. The matter forms an accretion disk around the primary star and accretes on it through the disk.

Dwarf novae (DNe) are a subclass of CVs and have out-

bursts of typically 2–5 mag. Their outbursts continue for days or weeks. The interval between outbursts are from several days to tens of years. The outbursts are understood as a sudden release of gravitational energy by a sudden increase of the mass accretion rate, which is caused by a thermal instability in the disk (see Warner 1995 for a review).

SU UMa-type DNe with short orbital periods (~ 1 hr $< P_{\text{orb}} < \sim 2$ hr) show occasional superoutbursts which are defined as outbursts with superhumps. The superhumps

are believed to appear because of the 3:1 resonance tidal instability (Osaki 1989; Whitehurst 1988; Hirose, Osaki 1990; Lubow 1991a; Lubow 1991b). Kato et al. (2009) proposed that the superhumps are divided into three stages by the variations of the period and amplitude (see Figure 1 on the classification of superhumps).

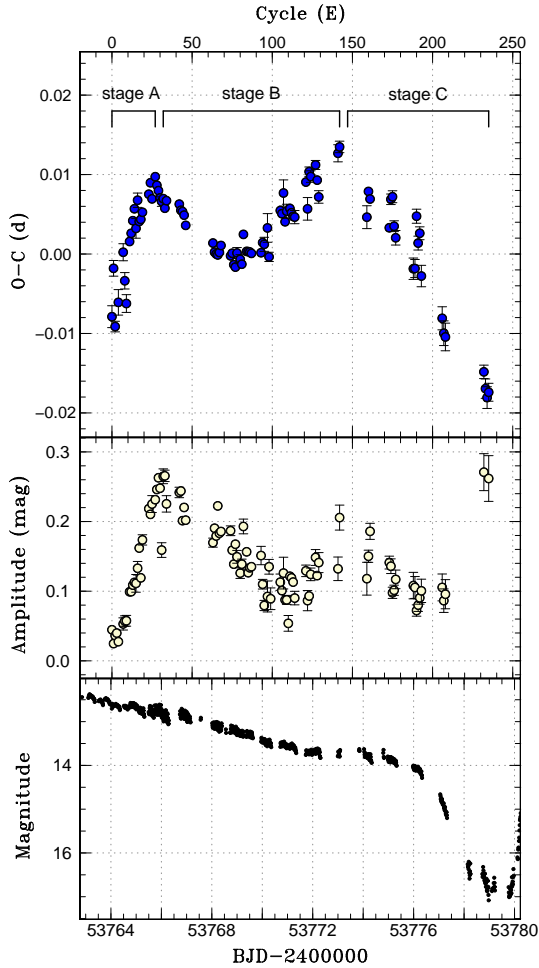


Fig. 1. Example of the classification of superhumps by the variations of the period and amplitude with the actual observational data of the 2006 outburst in ASAS J102522–1542.4, a WZ Sge-type star, derived from Fig. 24 of Kato et al. (2012). Upper panel: $O-C$ curve of the times of superhump maxima. Middle panel: amplitude of superhumps. Lower panel: light curve. The horizontal axis in units of BJD and cycle number of superhumps is common to these three panels.

WZ Sge-type DNe are an extreme subclass of SU UMa-type DNe, which predominantly show superoutbursts (for a review, Kato 2015). There are two important observational properties of them. One is the presence of double-peaked modulations called early superhumps having a period almost equal to the orbital one in the early stage of the superoutburst (Kato 2002; Ishioka et al. 2002). They are considered to be triggered by the 2:1 resonance tidal instability (Osaki, Meyer 2002; Osaki, Meyer 2003). The

other is rebrightening after the end of the plateau stage of the superoutburst. They classified the rebrightenings into five types according to the profiles of the light curves (Imada et al. 2006; Kato et al. 2009; Kato et al. 2014) (see Figure 2 on the classification of rebrightenings). The origin of the unique light curves is still an open question.

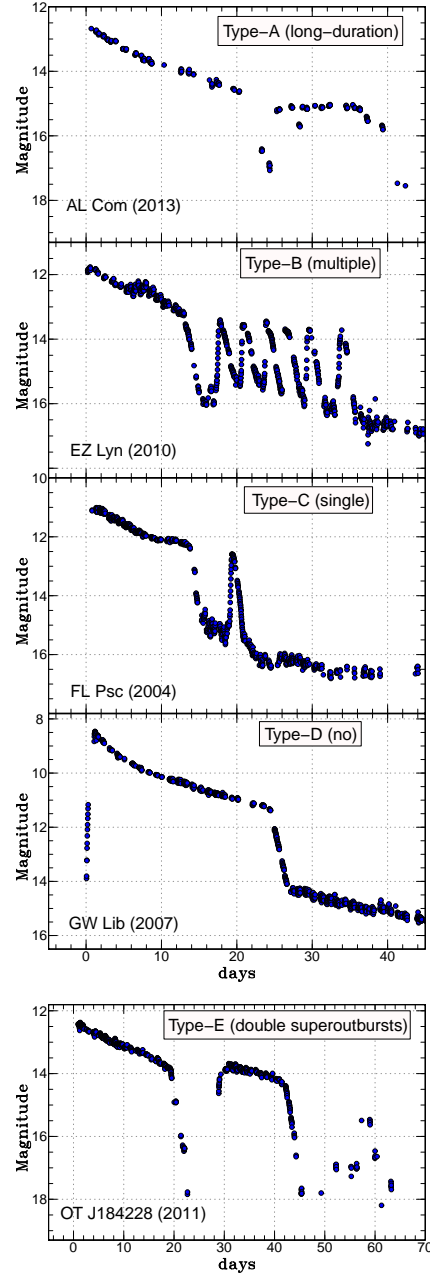


Fig. 2. Classification of rebrightenings by their morphology. We use the observational data in Fig. 6, 7, 8 and 9 of Kato (2015). The horizontal axis represents days from the starting date of their outbursts.

The evolutionary status of WZ Sge-type DNe is still in debate (e.g. Nakata et al. 2014). According to the

standard scenario of the CV evolution, CVs evolve as the orbital period becomes shorter because of angular momentum losses by magnetic braking and gravitational radiation. Once P_{orb} reaches the period minimum, the secondary star becomes degenerate and the thermal timescale of the secondary star becomes longer than the mass-transfer timescale. Hence, the systems evolve back toward longer orbital periods. They are called period bouncers (see Knigge et al. 2011 and references therein). Kolb (1993) suggested that $\sim 70\%$ of all CVs would be beyond the period minimum. It is however difficult to discover them because they are faint and have a long recurrence time between outbursts (Patterson 2011).

In the study of the missing population of post-period minimum CVs, it is worth noting that Littlefair et al. (2006) demonstrated with their spectroscopy that the donor star in the eclipsing CV SDSS J103533.03+055158.4 with a period close to the minimum one was a brown dwarf, suggesting that this object is a period bouncer. Moreover, Littlefair et al. (2008) found three more eclipsing CVs possess brown dwarfs as the secondary star using high-speed, three-color photometry. Recently, other several good candidates for a period bouncer have been discovered among WZ Sge-type DNe with type-B rebrightening or type-E rebrightening or slow fading rate (the objects and references are summarized in Table 1) through optical photometry using the new method of estimating the mass ratio (q) of the secondary to the primary with the period of stage A superhumps and the orbital period (Kato, Osaki 2013). These period-bouncer candidates have some common properties: (1) long-lasting stage A superhumps, (2) a large decrease of the superhump period between stage A and stage B, (3) a small superhump amplitude ($\lesssim 0.1$ mag) and (4) long-lasting early superhumps ($\gtrsim 10$ d). Kato (2015) also identified the relation between the rebrightening types and the CV evolutionary stage (WZ Sge-type stars would evolve in the order of type C \rightarrow D \rightarrow A \rightarrow B \rightarrow E) and the two objects with type-E rebrightening (see Table 1) are the best candidates for a period bouncer.

In this paper, we report on the optical photometry of a WZ Sge-type object, ASASSN-15jd having similar characteristics to those of the objects with type-E rebrightening. Its outburst was detected on 2015 May 13 by All-Sky Automated Survey for Supernovae (ASAS-SN) (Shappee et al. 2014; Davis et al. 2015). This object has a quiescent counterpart SDSS J164925.43+140243.5 ($g = 22.8$ mag) and its position is (RA:) 16h49m25.42s, (Dec:) +14°02′43.7″ (J2000.0).

This paper is structured as follows. We describe a log of observations and our analysis method in Section 2 and the results in Section 3. In Section 4, we discuss the results. A brief summary and further observations are described in Section 5.

2. Observation and Analysis

Time-resolved CCD photometry was carried out by the VSNET collaboration team at twelve sites (Table 2).

Table 3 shows the log of photometric observations. All of the observation times were converted to barycentric Julian date (BJD). Before making the analyses, we applied zero-point corrections to each observer by adding constants. The magnitude scales of each site were adjusted to that of the Kyoto University system (KU1 in Table 3), where GSC974.1416 (RA: 16h49m32.51s, Dec: +14°03′22.7″, $V = 13.0$) was used as the comparison star. The constancy of the comparison star was checked by nearby stars in the same images.

We used the phase dispersion minimization (PDM) method (Stellingwerf 1978) for a period analyses. We subtracted the global trend of the light curve by locally weighted polynomial regression (LOWESS: Cleveland 1979) before making the PDM analyses. The 1σ error of the best estimated period by the PDM analysis was determined by the methods in Fernie (1989) and Kato et al. (2010).

A variety of bootstraps was used for estimating the robustness of the result of PDM. We analyzed about 100 samples which randomly contained 50% of observations, and performed a PDM analysis for these samples. The result of the bootstrap is expressed as a form of 90% confidence intervals in the resultant θ statistics.

3. Results

3.1. Overall Light Curve

We show the overall light curve of the 2015 superoutburst of ASASSN-15jd in Figure 3. The superoutburst probably began on BJD 2457155 and the object showed a rapid rise at the very early stage. The first plateau stage continued for about ten days during BJD 2457155–2457164.4 and a small dip whose depth is about 1 mag was observed on BJD 2457165. Immediately after the dip, the object showed a rapid rise again and the second plateau stage started. It continued for about a week during BJD 2457165.2–2457172.4 and a rapid fading was seen on 2457174. There were no observations during BJD 2457178–2457186. On BJD 2457186, the onset of a rebrightening was detected (vsnet-alert 18815). The duration of the rebrightening was short, a few days.

3.2. Superhumps

During the dip (on BJD 2457165), ordinary superhumps started to develop. The $O - C$ curve of times of superhump maxima, the amplitude of superhumps and the light curve during BJD 2457165.2–2457172.4 are shown in the upper panel, the middle panel and the lower panel of Figure 4, respectively. We determined the times of maxima of ordinary superhumps in the same way as in Kato et al. (2009). Some points with large errors were removed in calculating the $O - C$ and amplitude. The resultant times are given in Table 4. Although we could not clearly identify the term of stage A only from the $O - C$ curve, we regarded BJD 2457166.2–2457167.6 ($0 \leq E \leq 16$) as the final part of stage A, judging from the variations of the superhump amplitudes. Also, we considered that the term of stage B was BJD 2457167.9–2457172.4 ($24 \leq E \leq 90$)

Table 1. Properties of candidates for a period bouncer

Object*	P_{orb}^{\dagger} (d)	P_1^{\ddagger} (d)	P_2^{\S} (d)	Amp	Profile of light curve [#]	Reference [¶]
MASTER J1222	0.059732(3)	0.06158(5)	0.060221(9)	0.0995	multiple rebrightenings (type-B)	1
MASTER J2037	0.06051(18)	0.06271(11)	0.061307(9)	0.114	multiple rebrightenings (type-B)	1
SSS J1222	0.075879(1)	0.07721(1)	0.07649(1)	0.115	double superoutbursts (type-E)	2
OT J1842	0.0724	0.07275**		0.08	double superoutbursts (type-E)	3
OT J0754	–	0.072218(3)	0.070758(6)	0.0531	slow decline	4
OT J2304	–	0.067245(17)	0.066351(12)	0.127	slow decline	4
ASASSN-14cv	0.059917(4)	0.06168(2)	0.060450(14)	0.0732	multiple rebrightenings (type-B)	5, 6
PNV J1714	0.059558(3)	0.06130(2)	0.060084(4)	0.0935	multiple rebrightenings (type-B)	5, 6
OT J0600	–	0.064659(12)	0.063310(4)	0.0648	multiple rebrightenings (type-B)	5, 6
ASASSN-15jd	–	–	0.064981(8)	0.0916	a small dip in the middle of the plateau	This paper

*Objects' name; MASTER J1222, MASTER J2037, SSS J1222, OT J1842, OT J0754, OT J2304, PNV J1714 and OT J0600 represent MASTER OT J211258.65+242145.4, MASTER OT J203749.39+552210.3, SSS J122221.7–311523, OT J184228.1+483742, OT J075418.7+381225, OT J230425.8+062546, PNV J17144255–2943481 and OT J060009.9+142615, respectively.

[†]Orbital period referring to the period of early superhumps.

[‡]Period of stage A superhumps.

[§]Period of stage B superhumps.

^{||}Mean amplitude of superhumps (mag).

[#]Characteristic shapes of light curves.

[¶]1: Nakata et al. (2013), 2: Kato et al. (2013), 3: Katysheva et al. (2013), 4: Nakata et al. (2014),

5: Nakata et al. in preparation, 6: Kato et al. (2015)

**Mean superhump period.

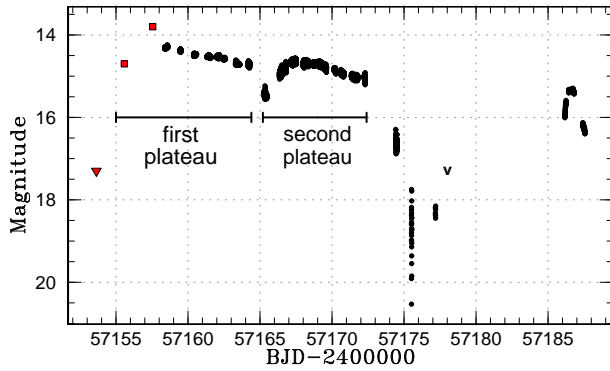


Fig. 3. Overall light curve of the 2015 superoutburst of ASASSN-15jd (BJD 2457153–2457188). The circles and ‘V’-shapes represent CCD photometric observations and upper limits by KU1 (ref. Table 3), respectively. The quadrangles and inverted triangles represent the detections and upper limits by ASAS-SN, respectively.

from the nonlinear behavior on the $O-C$ plane and the slow decrease of superhump amplitudes. The stage B superhumps might continue after BJD 2457172.4 although we could not detect it because of the sparse coverage. The superhumps disappeared at the fading stage on BJD 2457174 and did not develop again in the rebrightening at least in our low accuracy observations and we could not

find stage C during the second plateau stage and after that.

We applied a period analysis by the PDM method for stage B (BJD 2457167.9–2457172.4) and obtained a period of $P_{\text{sh}} = 0.0649810(78)$ d (see upper panel of Figure 5). Here, the data having low accuracy were excluded from the light curve when we performed our PDM analysis. The derivative of the superhump period during stage B was $P_{\text{dot}} (\equiv \dot{P}_{\text{sh}}/P_{\text{sh}}) = 10.8(3.8) \times 10^{-5} \text{ s}^{-1}$. The mean profile of stage B superhumps is also shown in the lower panel of Figure 5.

Early superhumps, double-wave modulations with a period almost the same as the orbital one usually appear prior to superhumps during superoutbursts of WZ Sge-type DNe (Kato 2002; Ishioka et al. 2002). However, during the first plateau stage of the 2015 outburst of ASASSN-15jd (during BJD 2457155–2457164.4), any humps with an amplitude of >0.02 mag were not observed in the range of 97.5–99.5% of the estimated superhump period in the previous paragraph.

In Figure 6, the daily variation of the profile of superhumps during BJD 2457165–2457172 is shown. The daily average amplitude of superhumps was 0.08–0.12 mag.

4. Discussion

4.1. Small Dip in the Plateau of the Superoutburst

ASASSN-15jd is the first example among WZ Sge-type DNe, which showed a small dip of brightness in the middle

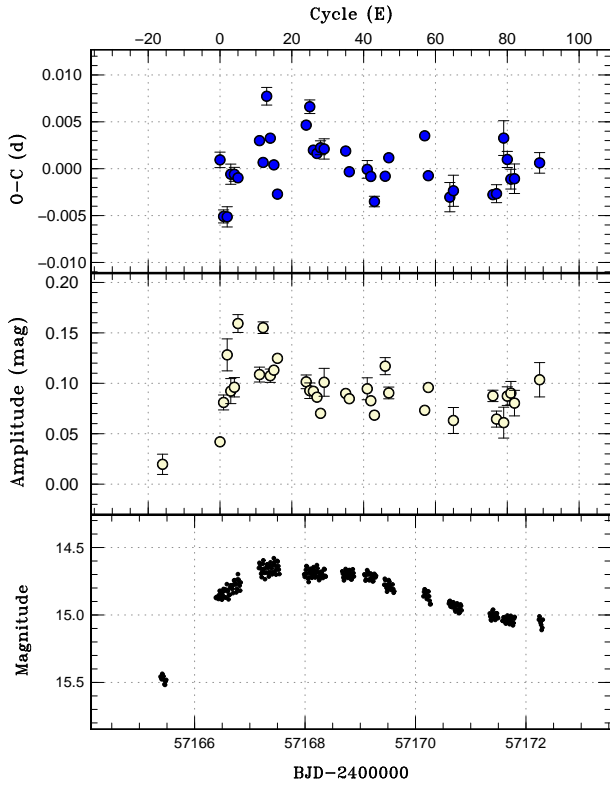


Fig. 4. Upper panel: $O - C$ curve of the times of superhump maxima of during BJD 2457165.2–2457172.4 (the second plateau stage of ASASSN-15jd). An ephemeris of BJD 2457166.459117+0.0650258 E was used for drawing this figure. Middle panel: amplitude of superhumps. Lower panel: light curve. The horizontal axis in units of BJD and cycle number is common to these three panels.

of the superoutburst. It has been known that the plateau stage of superoutbursts in WZ Sge-type objects can be classified into two types: single plateau stage observed in the objects with type-A, B, C and D rebrightening (except for type-E rebrightening) and double plateau stages observed only in the objects with type-E rebrightening. The schematic diagrams of the light curves of these two plateau types are depicted in Figure 7. The left and right panels of Figure 7 represent single plateau stage and double plateau stages, respectively. In the single plateau stage, ordinary superhumps are seen as soon as early superhumps disappear, while in the double plateau stages, ordinary superhumps begin to develop in the second plateau stage a few days after early superhumps disappear. The plateau stage in ASASSN-15jd cannot be classified as one of these two types of the plateau stage. There would be a possibility that the dip in ASASSN-15jd was deeper since we did not have adequate observations around the observed dip on BJD 2457165; nevertheless, the duration of the dip in this object was ~ 2 days and shorter than ~ 10 days duration in the objects with type-E rebrightening (Kato et al. 2013; Katysheva et al. 2013 and see also the bottom

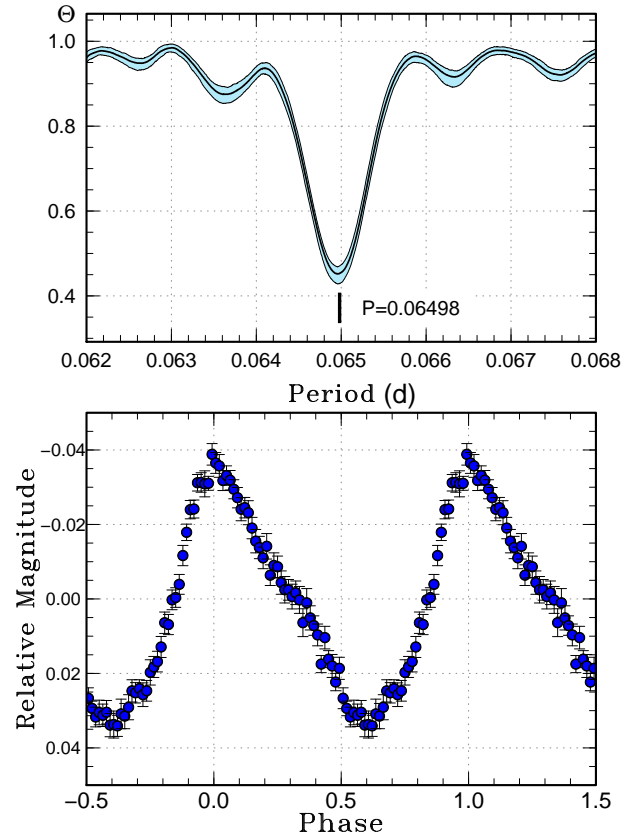


Fig. 5. Superhumps in the second plateau stage of the 2015 outburst of ASASSN-15jd. Upper: Θ -diagram of our PDM analysis of stage B superhumps (BJD 2457167.9–2457172.4). Lower: Phase-averaged profile of stage B superhumps.

panel of Figure 2). Hence, we can regard that ASASSN-15jd showed an intermediate light curve between the single plateau stage and the double ones.

Ordinary superhumps are considered to develop together with the 3:1 resonance tidal instability occurring in accretion disks (see e.g., Osaki 1996 for a theoretical review). We can therefore regard that the shapes of plateau stages in WZ Sge-type DNe reflect the speed at which the 3:1 resonance develops. In other words, it is considered that we cannot observe the dip of brightness in the plateau in the objects with the single plateau stage since the 3:1 resonance grows up as soon as the 2:1 resonance finishes working. In the cases when the 3:1 resonance does not grow sufficiently quickly, the cooling wave propagates in the accretion disk before the 3:1 resonance fully builds up in the objects with the double plateau stages, and hence, these have a dip of brightness. The 3:1 resonance in ASASSN-15jd seems to develop slower than that in the former objects (single plateau) and faster than that in the latter objects (double plateaus).

There is a theory explaining the reason why the delay in development of superhumps appears. The growth time of the 3:1 resonance tidal instability is inversely pro-

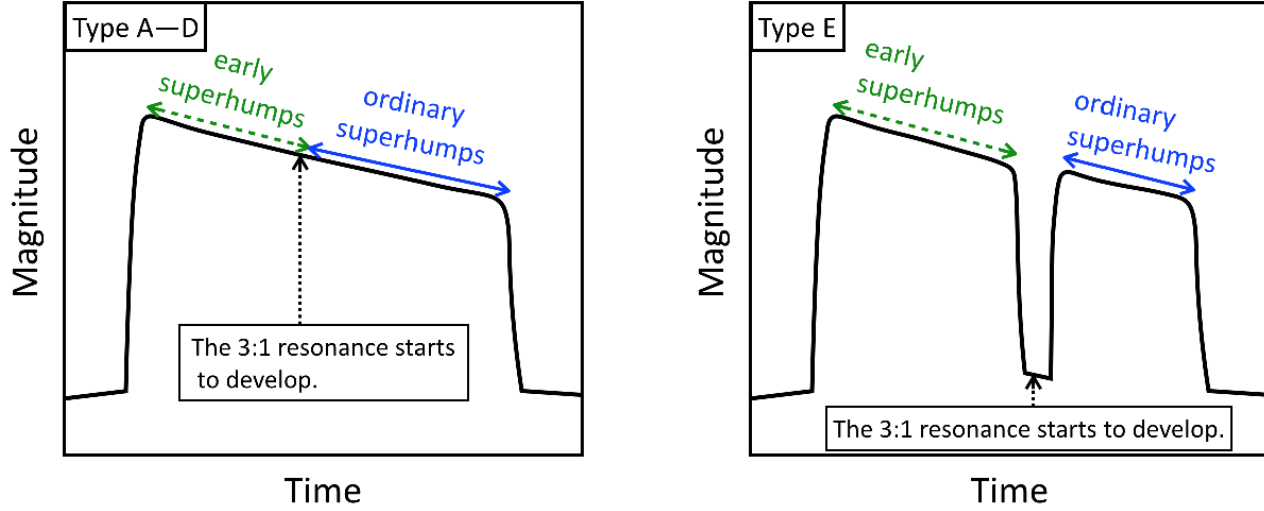


Fig. 7. Classification of plateau stages observed in WZ Sge-type DNe. Left: single plateau stage observed in objects with type-A, B, C and D rebrightenings. Right: double plateau stages observed in objects with type-E rebrightening.

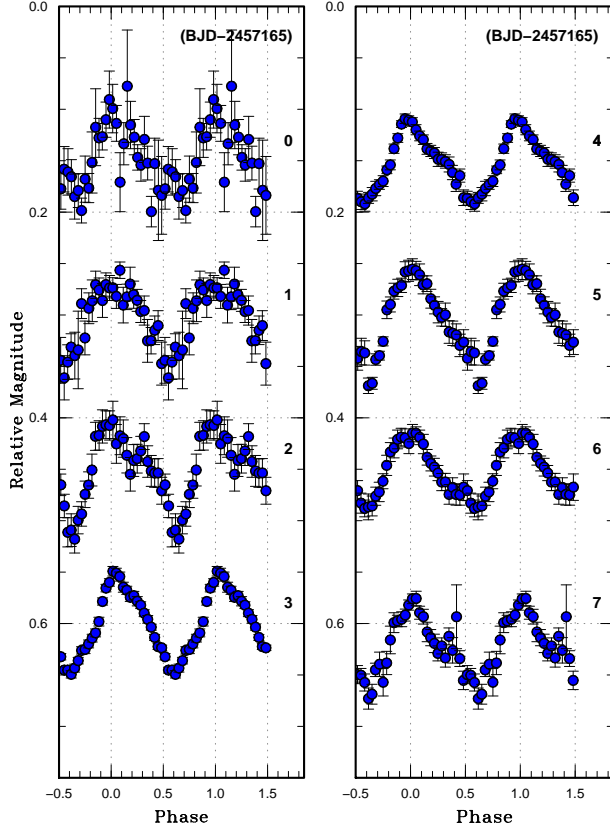


Fig. 6. Dairy variation of the profile of superhumps in ASASSN-15jd during BJD 2458165.2–2457172.4.

portional to the square of the mass ratio (Lubow 1991a). The type-E rebrightening was observed in the outbursts of SSS J122221.7–311523 and OT J184228.1+483742 in the past (Kato et al. 2013; Katysheva et al. 2013) and these

systems are considered to be promising candidates for a period bouncer because of their small estimated mass ratios (Kato 2015). Their mass ratios are smaller than those of other WZ Sge-type stars with the single plateau, and the behavior is consistent with the slow growth of the 3:1 resonance. Although we could not estimate the accurate value of the mass ratio of ASASSN-15jd, the 3:1 resonance seems to develop slower in this system than in WZ Sge-type stars with the single plateau stage judging from the shape of the plateau stage and it is expected that this object has a small q value. Combined with the relatively long P_{sh} for a WZ Sge-type star, ASASSN-15jd is likely to be a promising candidate for a period bouncer.

The rebrightening type after the second plateau stage in this outburst is probably C (single rebrightening) although there remain a possibility of multiple rebrightenings due to the lack of observations. This rebrightening type has been observed in many other WZ Sge-type objects.

4.2. Small Amplitude of Superhumps

The average superhump amplitude of ASASSN-15jd in the 2015 superoutburst was small, less than 0.1 mag (see the lower panel of Figure 5 and Figure 6). In about 90% of ordinary SU UMa-type DNe, the normalized superhump amplitudes fall within the range of 0.14–0.35 mag independent of the inclination (Kato et al. 2012).

We show the variation of superhump amplitudes of the SU UMa-type systems whose orbital periods are 0.06–0.07 d including ASASSN-15jd and the candidates for a period bouncer, in the left panel of Figure 8. In plotting this figure, we measured the amplitudes using the template fitting method described in Kato et al. (2009) and took zero of the cycle count from the start of stage B. In ASASSN-15jd, we regarded that the maximum amplitude on BJD 2457167 is at $E = 0$ for comparison since we could not clearly identify the start of stage B. Previous re-

search demonstrates that the mean superhump amplitude is small ($\lesssim 0.1$ mag) in the extreme WZ Sge-type systems which are the candidates for a period bouncer (see Table 1 for the details). From this figure, we can see the amplitudes in ASASSN-15jd are about two times smaller than those of ordinary SU UMa-type DNe and have about the same values as those in the best candidates for a period bouncer.

Additionally, in the right panel of Figure 8, we give the relation between maximum superhump amplitudes and orbital periods in SU UMa-type stars. The samples of ordinary SU UMa-type objects and period-bouncer candidates that we used in this figure are the objects listed in Table 73 of Kato et al. (2012) and Table 1 of this paper, respectively. In this figure, we substituted the stage B superhump period and the average superhump period for the orbital periods in OT J060009.9+142615 and ASASSN-15jd, respectively. The mean maximum amplitude in the objects which have $P_{\text{orb}} = 0.065$ is about 0.25 mag, but, that in ASASSN-15jd is 0.091. In addition, the maximum amplitudes in the best candidates for a period bouncer are also small and out of the distribution of ordinary SU UMa-type DNe.

Therefore, the small superhump amplitude in ASASSN-15jd can be regarded as the representation of the characteristic properties of a period bouncer. The properties of the candidates for a period bouncer are summarized in Table 1.

4.3. Absence of Early Superhumps

In ASASSN-15jd, no ordinary superhumps were observed for about ten days from the onset of the outburst to the small dip of brightness (on BJD 2457165). In addition, we could not detect early superhumps for that term although they are usually observed in outbursts of WZ Sge-type stars for about a week (Kato 2015) before ordinary superhumps develop. Uemura et al. (2012) proposed that early superhumps are caused by the rotation effect of non-axisymmetrically flaring accretion disks (see also Nogami et al. 1997 and Kato 2002). High-inclination (edge-on) systems thus tend to show large-amplitude early superhumps. In addition, early superhumps are regarded as the manifestation of the 2:1 resonance tidal instability and the 2:1 resonance is considered to suppress the development of ordinary superhumps (Lubow 1991a; Osaki, Meyer 2002; Osaki, Meyer 2003). Based on the above theories, we suggest that the inclination angle of ASASSN-15jd is low and we observed this system at nearly face-on from our results: 1) the superhumps start to develop at the dip, 2) neither early superhumps nor ordinary ones were observed before the dip

Note that the duration for which the 2:1 resonance supposed to have been dominant before the superhumps developed in ASASSN-15jd is longer than the average duration of early superhumps in ordinary WZ Sge-type DNe. In the superoutbursts of the promising candidates for a period bouncer, the durations of the early superhumps were usually long and this can be one of characters of period bouncers (Kato et al. 2013; Nakata et al. 2013; Nakata et

al. in preparation). Therefore, this finding suggests that ASASSN-15jd has yet another property common to period bouncers.

5. Summary

We have reported on our photometric observations of a WZ Sge-type DN, ASASSN-15jd. What we found on this object from our observations is as follows:

- ASASSN-15jd is the first WZ Sge-type object with a small dip of brightness in the middle of the superoutburst. This implies that the 3:1 resonance grew up slowly in its outburst and the mass ratio is considered to be small.
- The superhump amplitude in ASASSN-15jd was small and the mean value was less than 0.1 mag.
- The inclination angle of ASASSN-15jd may be low judging from the lack of early superhumps. The interval without ordinary superhumps was relatively long, about ten days.

We suggest that ASASSN-15jd would be a promising candidate for a period bouncer because the above properties are very similar to those of other best candidates for a period bouncer. Gänsicke et al. (2009) reported that the optical spectra of SDSS CVs whose orbital periods are close to the minimum one are dominated by emission from the white dwarf photosphere and that the contribution to the spectra from the companion star is no or little. This means that they have very low mass companion stars, in other words, they have very small mass ratios. Hence, spectroscopic observation of ASASSN-15jd may be useful to confirm its low mass ratio.

Acknowledgements

This work was supported by a Grant-in-Aid ‘‘Initiative for High-Dimensional Data-Driven Science through Deepening of Sparse Modeling’’ from the Ministry of Education, Culture, Sports, Science and Technology (MEXT) of Japan (25120007). Also, it was partially supported by the RFB grant 15-02-06178. We appreciate All-Sky Automated Survey for Supernovae (ASAS-SN) detecting a large amount of DNe. We are thankful to many amateur observers for providing a lot of data used in this research.

Supporting information

Additional supporting information can be found in the online version of this article: Supplementary tables 2, 3 and 4.

Supplementary data is available at PASJ Journal online (*included at the end in this astro-ph version*).

References

Cleveland, W. S. 1979, J. Amer. Statist. Assoc., 74, 829

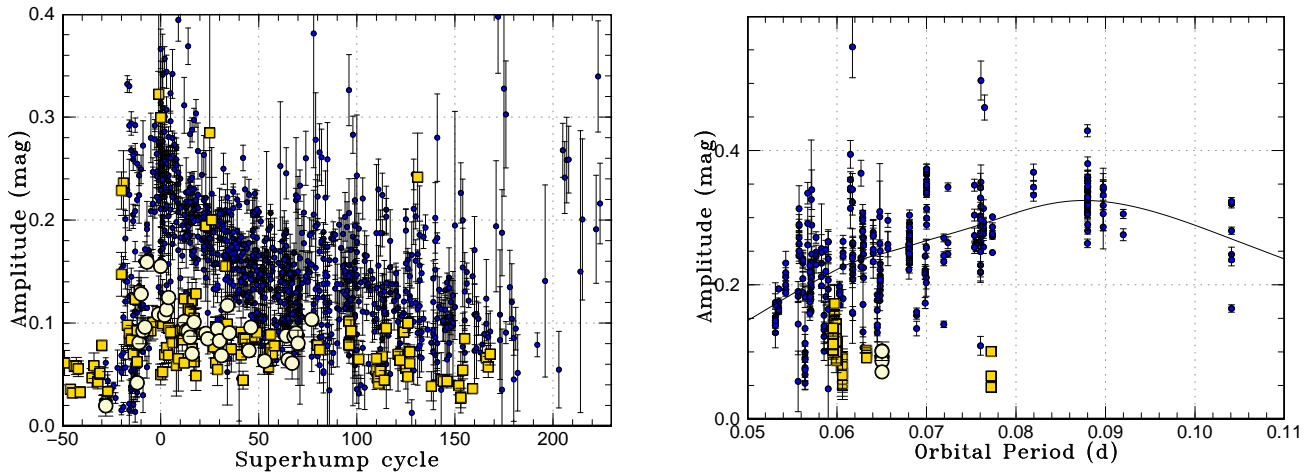


Fig. 8. Left: Variation of superhump amplitudes in the SU UMa-type objects with $0.06 \text{ d} < P_{\text{orb}} \leq 0.07 \text{ d}$. Open circles and rectangles represent our results in ASASSN-15jd and the amplitudes of the candidates for a period bouncer, respectively. Other data indicated by filled circles are the same as in Fig. 87 of Kato et al. (2012). Right: Dependence of superhump amplitudes on orbital periods (the relation between the maximum superhump amplitudes and the orbital period). Open circles and rectangles represent the same as in the left panel. Filled circles indicate the amplitudes of ordinary SU UMa-type systems got from Fig. 89 of Kato et al. (2012). We selected epochs $5 < E < 10$ to illustrate the maximum superhump amplitudes. The curve indicates a spline-smoothed interpolation of the data of ordinary SU UMa-type stars.

- Davis, A. B., Shappee, B. J., Archer Shappee, B., & ASAS-SN 2015, American Astron. Soc. Meeting Abstracts, 225, #344.02
- Fernie, J. D. 1989, PASP, 101, 225
- Gänsicke, B. T., et al. 2009, MNRAS, 397, 2170
- Hirose, M., & Osaki, Y. 1990, PASJ, 42, 135
- Imada, A., Kubota, K., Kato, T., Nogami, D., Maehara, H., Nakajima, K., Uemura, M., & Ishioka, R. 2006, PASJ, 58, L23
- Ishioka, R., et al. 2002, A&A, 381, L41
- Kato, T. 2002, PASJ, 54, L11
- Kato, T. 2015, PASJ, 67, 108
- Kato, T., et al. 2015, PASJ, 67, 105
- Kato, T., et al. 2014, PASJ, 66, 30
- Kato, T., et al. 2009, PASJ, 61, S395
- Kato, T., et al. 2012, PASJ, 64, 21
- Kato, T., et al. 2010, PASJ, 62, 1525
- Kato, T., Monard, B., Hamsch, F.-J., Kiyota, S., & Maehara, H. 2013, PASJ, 65, L11
- Kato, T., & Osaki, Y. 2013, PASJ, 65, 115
- Katysheva, N., et al. 2013, Central European Astrophys. Bull., 37, 335
- Knigge, C., Baraffe, I., & Patterson, J. 2011, ApJS, 194, 28
- Kolb, U. 1993, A&A, 271, 149
- Littlefair, S. P., Dhillon, V. S., Marsh, T. R., Gänsicke, B. T., Southworth, J., Baraffe, I., Watson, C. A., & Copperwheat, C. 2008, MNRAS, 388, 1582
- Littlefair, S. P., Dhillon, V. S., Marsh, T. R., Gänsicke, B. T., Southworth, J., & Watson, C. A. 2006, Science, 314, 1578
- Lubow, S. H. 1991a, ApJ, 381, 259
- Lubow, S. H. 1991b, ApJ, 381, 268
- Nakata, C., et al. 2014, PASJ, 66, 116
- Nakata, C., et al. 2013, PASJ, 65, 117
- Nogami, D., Kato, T., Baba, H., Matsumoto, K., Arimoto, J., Tanabe, K., & Ishikawa, K. 1997, ApJ, 490, 840
- Osaki, Y. 1989, PASJ, 41, 1005
- Osaki, Y. 1996, PASP, 108, 39
- Osaki, Y., & Meyer, F. 2002, A&A, 383, 574
- Osaki, Y., & Meyer, F. 2003, A&A, 401, 325
- Patterson, J. 2011, MNRAS, 411, 2695
- Shappee, B. J., et al. 2014, ApJ, 788, 48
- Stellingwerf, R. F. 1978, ApJ, 224, 953
- Uemura, M., Kato, T., Ohshima, T., & Maehara, H. 2012, PASJ, 64, 92
- Warner, B. 1995, Cataclysmic Variable Stars (Cambridge: Cambridge University Press)
- Whitehurst, R. 1988, MNRAS, 232, 35

Table 2. List of Instruments

CODE*	Telescope (& CCD)	Observatory (or Observer)	Site
CRI	38cm K-380+Apogee E47	Crimean astrophysical observatory	Crimea
DPV	28cmSC+MII G2-1600	Astronomical Obs. on Kolonica Saddle	Slovakia
	35cmSC+MII G2-1600	Astronomical Obs. on Kolonica Saddle	Slovakia
	VNT 1m+FLI PL1001E	Astronomical Obs. on Kolonica Saddle	Slovakia
Ter	Zeiss-600 60cm	Terskol Observatory	Russia
	S2C 35cm	Terskol Observatory	Russia
RPc	FTN 2.0m+E2V 42-40	LCOGT [†]	Hawaii, USA
	35cmSC+SXV-H9 CCD	Roger D. Pickard	UK
Trt	25cm ALCCD5.2 (QHY6)	Tamás Tordai	Budapest, Hungary
KU1	40cmSC+ST-9XEI	Kyoto U. Team	Kyoto, Japan
SWI	C14 35cmSC+ST10XME	William L. Stein	New Mexico, USA
OKU	51cm+Andor DW936N-BV	OKU Astronomical Observatory	Osaka, Japan
IMi	35cmSC+SXVR-H16	Ian Miller	Furzehill Observatory
Van	35cmSC+SBIG ST-7XME CCD	CBA Belgium Observatory	Belgium
DKS	LX200 25cm	Rolling Hills Observatory	USA
Ioh	30cmSC+ST-9XE CCD	Hiroshi Itoh	Tokyo, Japan

*see the annotation in Table 3

[†]Las Cumbres Observatory Global Telescope Network

Table 3. Log of observations of ASASSN-15jd in 2015

Start*	End*	Mag [†]	Error [‡]	N^{\S}	Obs	Band [#]	exp[s]
58.3835	58.5979	14.300	0.002	173	Van	<i>C</i>	60
59.4360	59.5155	14.386	0.002	93	Van	<i>C</i>	60
60.3841	60.5916	14.484	0.001	227	Van	<i>C</i>	60
61.3155	61.5612	14.523	0.001	306	DPV	<i>C</i>	60
61.3888	61.5035	14.517	0.001	153	Trt	<i>C</i>	60
61.5031	61.5974	14.540	0.001	95	Van	<i>C</i>	60
62.0047	62.1933	14.530	0.001	492	KU1	<i>C</i>	30
62.1640	62.1899	14.500	0.001	70	OKU	<i>C</i>	30
62.4018	62.5906	14.571	0.001	192	Van	<i>C</i>	60
62.4563	62.5377	14.576	0.001	150	IMi	<i>CV</i>	30
63.2956	63.4021	14.674	0.002	100	CRI	<i>C</i>	120
63.3849	63.5911	14.707	0.001	231	Van	<i>C</i>	60
64.1458	64.2850	14.706	0.002	275	KU1	<i>C</i>	30
64.1566	64.2693	14.732	0.001	156	OKU	<i>C</i>	30
65.2691	65.3961	15.423	0.009	61	CRI	<i>C</i>	120
65.3866	65.4792	15.476	0.003	107	Van	<i>C</i>	60
66.3356	66.5482	14.906	0.006	145	CRI	<i>C</i>	120
66.3865	66.5916	14.844	0.003	195	Van	<i>C</i>	60
66.4446	66.5118	14.843	0.002	126	IMi	<i>CV</i>	30
66.5903	66.8343	14.787	0.003	268	DKS	<i>C</i>	60
67.1612	67.2776	14.661	0.004	149	OKU	<i>C</i>	30
67.2943	67.5335	14.655	0.004	110	CRI	<i>C</i>	120
67.3753	67.5206	14.643	0.002	359	Ter	<i>C</i>	30
67.9861	68.2617	14.690	0.001	719	KU1	<i>C</i>	30
68.1661	68.2851	14.695	0.002	318	OKU	<i>C</i>	30
68.2725	68.3749	14.696	0.003	73	CRI	<i>C</i>	120
68.6699	68.8851	14.700	0.002	272	SWI	<i>C</i>	60
69.0767	69.2842	14.960	0.002	288	Ioh	<i>C</i>	60
69.1712	69.2695	14.722	0.001	246	OKU	<i>C</i>	30
69.4363	69.5539	14.777	0.002	228	IMi	<i>CV</i>	30
69.5811	69.6179	14.812	0.006	52	RPc	<i>V</i>	60
70.1466	70.2738	14.856	0.002	336	OKU	<i>C</i>	30
70.6038	70.8384	14.938	0.002	279	DKS	<i>C</i>	60
71.3427	71.4869	15.007	0.002	186	DPV	<i>C</i>	60
71.3710	71.4926	15.002	0.003	169	Trt	<i>C</i>	60
71.5756	71.7965	15.039	0.002	256	DKS	<i>C</i>	60
72.2365	72.3010	15.061	0.005	141	KU1	<i>C</i>	30
74.4216	74.5255	16.666	0.010	114	RPc	<i>CV</i>	60
75.5129	75.5338	18.999	0.159	28	DPV	<i>C</i>	60
77.1767	77.1926	18.298	0.036	9	OKU	<i>C</i>	30
86.1662	86.2473	15.812	0.019	40	OKU	<i>C</i>	30
86.4214	86.5462	15.364	0.001	128	Van	<i>C</i>	60
86.6490	86.8169	15.360	0.002	215	SWI	<i>C</i>	120
87.4142	87.5649	16.265	0.006	128	Van	<i>C</i>	60

*BJD – 2457100.0.

†Mean magnitude.

‡ 1σ of mean magnitude.

§Number of observations.

||Observer's code: Van (Tonny Vanmunster), DPV (Pavol A. Dubovsky),

Trt (Tamás Tordai), KU1 (Kyoto Univ. Team),

OKU (Osaka Kyoiku Univ. Team), IMi (Ian Miller),

CRI (Crimean Observatory Team), DKS (Shawn Dvorak)

Ter (Terskol Observatory), SWI (William L. Stein) Ioh (Hiroshi Itoh),

and RPc (Roger D. Pickard)

#Filter. “V” means V filter, “C” and CV mean no filter (clear).

Table 4. Times of superhump maxima in ASASSN-15jd

E	Max [†]	Error	$O - C$ [‡]	N [§]
0	57166.4601	0.0008	0.0009	136
1	57166.5191	0.0007	-0.0051	84
2	57166.5840	0.0011	-0.0051	56
3	57166.6536	0.0011	-0.0006	64
4	57166.7186	0.0007	-0.0006	60
5	57166.7833	0.0004	-0.0010	63
11	57167.1774	0.0004	0.0030	59
12	57167.2401	0.0003	0.0007	61
13	57167.3122	0.0009	0.0077	21
14	57167.3727	0.0005	0.0033	87
15	57167.4349	0.0003	0.0004	154
16	57167.4968	0.0003	-0.0027	136
24	57168.0244	0.0005	0.0047	137
25	57168.0914	0.0007	0.0066	131
26	57168.1518	0.0004	0.0020	169
27	57168.2164	0.0003	0.0016	274
28	57168.2821	0.0007	0.0022	121
19	57168.3470	0.0011	0.0021	36
35	57168.7369	0.0004	0.0019	63
36	57168.7997	0.0004	-0.0003	68
41	57169.1251	0.0009	-0.0001	72
42	57169.1894	0.0004	-0.0008	177
43	57169.2517	0.0006	-0.0035	189
46	57169.4495	0.0004	-0.0008	77
47	57169.5165	0.0005	0.0012	99
57	57170.1691	0.0004	0.0035	126
58	57170.2299	0.0003	-0.0007	139
64	57170.6177	0.0016	-0.0030	44
65	57170.6834	0.0017	-0.0024	64
76	57171.3983	0.0005	-0.0028	140
77	57171.4634	0.0010	-0.0027	133
79	57171.5994	0.0019	0.0033	60
80	57171.6622	0.0009	0.0010	65
81	57171.7251	0.0011	-0.0011	56
82	57171.7902	0.0016	-0.0011	38
89	57172.2470	0.0011	0.0006	79

*Cycle counts.

†BJD-2400000.0.

‡ $C = 2457166.459117 + 0.0650258 E$.

§Number of points used for determining the maximum.